forests

MDPI

Article

Tropical Forest Disturbance Monitoring Based on Multi-Source Time Series Satellite Images and the LandTrendr Algorithm

Xiong Yin [1,2], Weili Kou [2,*], Ting Yun [3], Xiaowei Gu [1,2], Hongyan Lai [1,2], Yue Chen [2], Zhixiang Wu [1] and Bangqian Chen [1,*]

[1] Rubber Research Institute (RRI), Chinese Academy of Tropical Agricultural Sciences (CATAS), Hainan Danzhou Agro-Ecosystem National Observation and Research Station, State Key Laboratory Incubation Base for Cultivation & Physiology of Tropical Crops, Haikou 571101, China
[2] College of Big Data and Intelligence Engineering, Southwest Forestry University, Kunming 650224, China
[3] College of Forestry, Nanjing Forestry University, Nanjing 210037, China
* Correspondence: kwl_eric@163.com (W.K.); chbq40@163.com (B.C.)

Abstract: Monitoring disturbances in tropical forests is important for assessing disturbance-related greenhouse gas emissions and the ability of forests to sequester carbon, and for formulating strategies for sustainable forest management. Thanks to a long-term observation history, large spatial coverage, and support from powerful cloud platforms such as Google Earth Engine (GEE), remote sensing is increasingly used to detect forest disturbances. In this study, three types of forest disturbances (abrupt, gradual, and multiple) were identified since the late 1980s on Hainan Island, the largest tropical island in China, using an improved LandTrendr algorithm and a dense time series of Landsat and Sentinel-2 satellite images on the GEE cloud platform. Results show that: (1) the algorithm identified forest disturbances with high accuracy, with the R^2 for abrupt and gradual disturbance detection reaching 0.92 and 0.83, respectively; (2) the total area in which forest disturbances occurred on Hainan Island over the past 30 years accounted for 10.84% (2.33×10^5 hm^2 in total area, at 0.35% per year) of the total forest area in 2020 and peaked around 2005; (3) the areas of abrupt, gradual, and multiple disturbances were 1.21×10^5 hm^2, 9.96×10^4 hm^2, and 1.25×10^4 hm^2, accounting for 51.93%, 42.75%, and 5.32% of the total disturbed area, respectively; and (4) most forest disturbance occurred in low-lying (<600 m elevation accounts for 97.42%) and gentle (<25° slope accounts for 94.42%) regions, and were mainly caused by the rapid expansion of rubber, eucalyptus, and tropical fruit plantations and natural disasters such as typhoons and droughts. The resulting algorithm and data products provide effective support for assessments of such things as tropical forest productivity and carbon storage on Hainan Island.

Keywords: Hainan Island; forest disturbances; LandTrendr; Google Earth engine

Citation: Yin, X.; Kou, W.; Yun, T.; Gu, X.; Lai, H.; Chen, Y.; Wu, Z.; Chen, B. Tropical Forest Disturbance Monitoring Based on Multi-Source Time Series Satellite Images and the LandTrendr Algorithm. *Forests* **2022**, *13*, 2038. https://doi.org/10.3390/f13122038

Academic Editor: José Aranha

Received: 19 October 2022
Accepted: 28 November 2022
Published: 30 November 2022

1. Introduction

Forest disturbance is one of the most important processes in forest ecosystem succession and plays an integral role in maintaining regional ecological balance and stability [1]. However, due to the increasing frequency of human and natural disturbances, forest structure and function have changed significantly, particularly in tropical forests, which are important contributors to the global carbon cycle and biodiversity [2,3]. It is estimated that about 55% of the global forest carbon stock is stored in tropical forests, which host approximately two-thirds of global biodiversity hotspots [4,5]. Therefore, information on the location, timing, and magnitude of disturbances in tropical forests must be quantified to understand forest disturbance processes and develop strategies to mitigate the resulting negative impacts [6–8].

Field surveys are a traditional method for the high-precision monitoring of forest disturbances, but they are time consuming, labor intensive, and limited in terms of time and space [9]. In contrast, remote sensing is a practical solution for forest disturbance monitoring because it allows rapid image acquisition, provides large spatial coverage, and is widely used to monitor forest disturbances caused by human-induced (logging [10,11], disforest), natural (fire [12,13], drought [14,15], pests and diseases [10,16]), or unknown factors [17–19]. Developing or selecting an appropriate disturbance monitoring algorithm is a key step in forest disturbance monitoring. Several forest disturbance monitoring algorithms based on long-term Landsat imagery have been developed in recent decades, including Landsat-based Detection of Trends in Disturbance and Recovery (LandTrendr) [20], Vegetation Change Tracker (VCT) [21], Breaks for Additive Season and Trend Monitor (BFAST) [22], and the Continuous Change Detection and Classification (CCDC) model [23]. These algorithms use pixels as the minimum mapping unit, and there are differences in the required temporal frequencies (number of remote sensing images used for the same location), change indices (spectral bands, vegetation indices, tasseled cap transformations), and whether they can be used for real-time monitoring [24]. The LandTrendr algorithm is flexible in the selection of vegetation indices, and can capture both abrupt and gradual disturbances [20]. Moreover, in tropical areas that are often affected by cloud cover and rainfall, the algorithm can freely define the time window to create composite cloud-free images, giving it wider adaptability [25]. A growing number of studies have subsequently proven the accuracy of the LandTrendr algorithm for monitoring forest disturbances (e.g., [26,27]). Additionally, since the implementation of the LandTrendr algorithm on the Google Earth Engine (GEE) cloud platform in 2018, the advantages of cloud computing have made it possible to efficiently monitor changes in forest disturbances at large scales [28,29].

Although the LandTrendr algorithm is widely used in forest disturbance monitoring, a literature review showed that there are still some shortcomings. First, most studies rely solely on Landsat imagery, with few using a combination of multiple data sources. Frequent rainfall and cloud cover in the tropics significantly hinder the acquisition of cloud-free Landsat imagery [30], reducing the accuracy of forest disturbance monitoring. With the launch of Sentinel-2A in June 2015, and with free data sharing, image coverage in the tropics has been greatly improved. The combination of Landsat and Sentinel-2 imagery can provide denser time series data for monitoring forest disturbances in the tropics [31]. Second, previous studies have monitored the most recent forest disturbances, ignoring the fact that forest disturbances often have multiple dynamics, such as eucalypt plantations with constant crop rotation. Timely determination of the timing and intensity of each disturbance, whether abrupt disturbances with short disturbance durations such as logging and fire or gradual disturbances with long disturbance durations such as selective logging and droughts, has important implications for sustainable forest management and the study of the carbon cycle [32–34].

Hainan Island is one of the two major tropical regions in China. It has a large area of tropical forests and is one of the world's biodiversity hotspots [2,35,36]. Existing studies have shown that the area and structure of the tropical forests on Hainan Island have changed drastically in recent decades. Forestry survey data show that forest cover has increased rapidly from 25.55% in 1987 to 49.15% in 2003, and the area of forest plantations accounts for 65.46% of the total forest area [37]. In the mid-to-late 1990s, under the promotion of the government, the planting area of eucalyptus increased rapidly [38]. Since the beginning of this century, the area of rubber plantations has increased rapidly in conjunction with the rapid rise in natural rubber prices, from 3.70×10^5 hectares in 2000 to 5.19×10^5 hectares in 2020 [39]. Wang, et al. in 2012 [40] evaluated several periods of satellite imagery and found that natural forest area increased significantly from 1988 to 1998, but decreased significantly from 1998 to 2008. A more recent study combining a dense time series of optical and synthetic aperture radar imagery (SAR) showed that the rapid expansion of rubber plantations since the 2000s contributed to a substantial increase in forest area between 2007 and 2018 [35]. However, these studies mainly analyzed forest changes on Hainan Island using statistical data or various forest distribution maps and lacked long-term monitoring of the type and intensity of forest disturbances, which greatly affected the comprehensive assessment of the forest dynamics on Hainan Island. The objectives of this study are threefold: (1) to identify different forest disturbances (abrupt disturbances, gradual disturbances, and multiple disturbances) using a dense time series of Landsat and Sentinel-2 imagery and the LandTrendr algorithm; (2) to analyze the spatiotemporal characteristics of forest disturbances on Hainan Island; and (3) to investigate the causes of different forest disturbances. The algorithms and data products obtained in this study can contribute to the sustainable management of forests on Hainan Island.

2. Method

2.1. Study Area

Hainan Island (108°21′–111°03′ E, 18°20′–20°10′ N) is the southernmost province of China and the second-largest island in the country, covering a land area of about 3.54×10^6 hectares (Figure 1). The topography of the island is low all around and high in the middle, with Wuzhi Mountain and Yinggeling in the middle, and slopes in all directions. Hainan Island belongs to the tropical monsoon climate zone with an average annual temperature of 22 to 27 degrees. The total annual rainfall ranges from 923 mm to 2459 mm and is mainly concentrated in the rainy season, which begins in May and lasts until October. Every year during the rainy season, forests and crops on the island are threatened by typhoons or severe tropical cyclones of varying intensity. The dry season generally lasts from November to April, and the amount of rainfall is about 20% of that occurring in the rainy season [41].

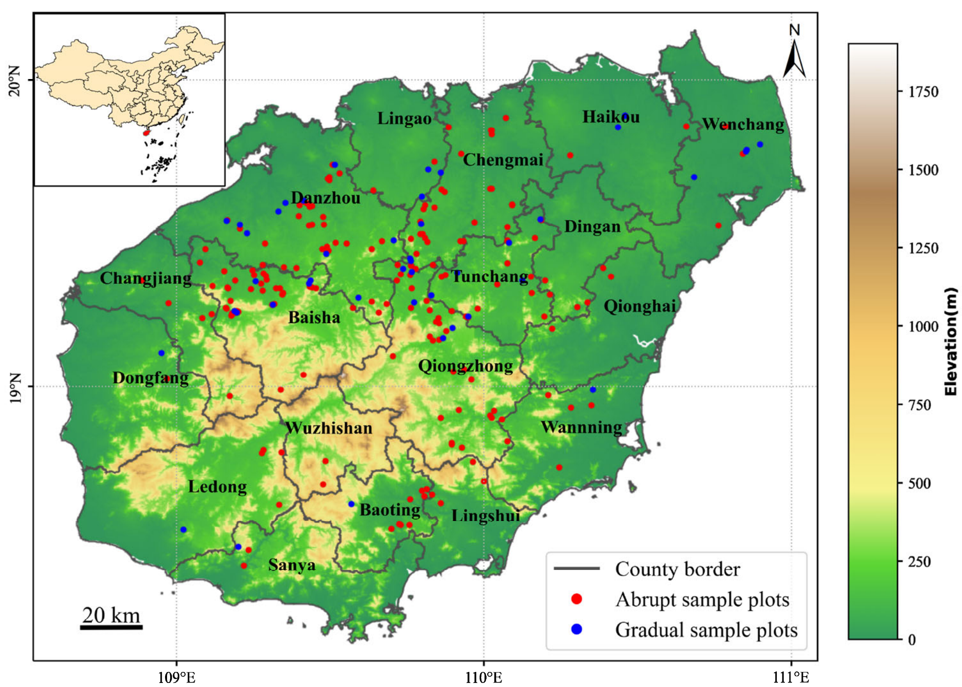

Figure 1. Spatial distribution map of topographic and ground samples on Hainan Island.

Hainan Island is extremely rich in forest resources, including tropical monsoon forests, tropical rainforests, evergreen broad-leaved forests, coniferous forests, and shrubs. According to the National Forest Resource Inventory, the forest cover of Hainan Island has increased from 31.27% in the fourth survey (1989–1993) to 57.36% in the ninth survey (2014–2018), ranking sixth among all provinces in China. The region is also subject to a variety of natural (typhoons, rainstorms, droughts) and human-induced (harvests, logging, clearings for agriculture, city construction) disturbances.

2.2. Workflow

The main process of this study consists of four steps (Figure 2): (1) synthesizing an annual time series dataset using Landsat and Sentinel-2 imagery from 1987 to 2020; (2) combining the forest map of Hainan Island in 2020 and the LandTrendr algorithm to identify different types of forest disturbances (abrupt disturbances, gradual disturbances, and multiple disturbances); (3) evaluating the accuracy of the different forest disturbances; and (4) analyzing the driving factors of the forest disturbances.

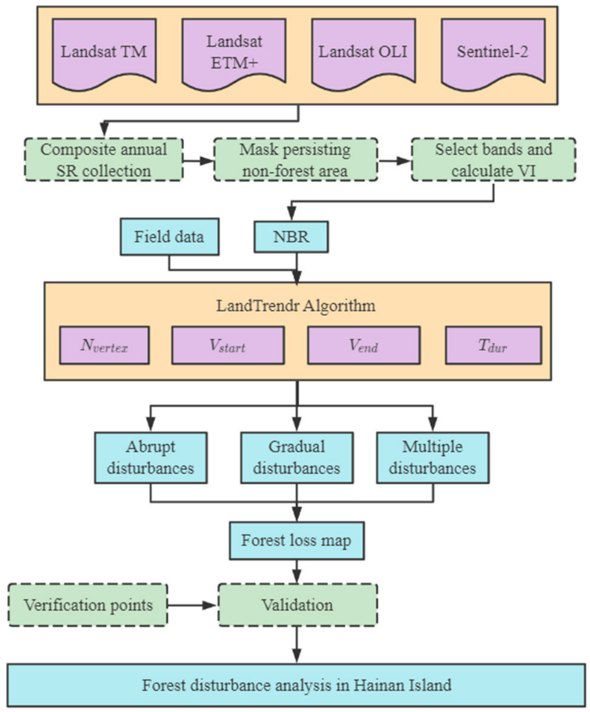

Figure 2. Workflow of this study.

2.3. Data Source and Processing

2.3.1. Satellite Imagery

All top-of-atmosphere (TOA) reflectance data acquired from the Landsat 5 Thematic Mapper (TM), Landsat 7 Enhanced Thematic Mapper Plus (ETM+), Landsat 8 Operational Land Imager (OLI), and Sentinel-2 Multispectral Instrument (MSI) were used to monitor forest disturbances. Hainan Island has a large number of rubber forests which lose their leaves intensively around mid-February every year, at which point the vegetation index drops significantly, and this can be easily misidentified as a forest disturbance. Therefore, we used the annual time series composite images created from 15 April to 30 November every year [42,43]. The Landsat imagery is from the U.S. Geological Survey, while the Sentinel-2 imagery is from the European Space Agency. These data are already corrected with high geometric precision, reducing radiometric uncertainties between different acquisition dates and sensors. All data are available on the Google Earth Engine cloud platform [44,45].

Clouds and shadows in the Landsat imagery were masked using bitmask information from the corresponding quality assessment band generated using the C Function of Mask (CFMask) algorithm [46,47],, while in the Sentinel-2 MSI images, these were masked using the cloud probability layer and the Temporal Dark Outlier Mask (TDOM) algorithm [46–48]. Regression models were used to minimize the differences in TOA reflectance between the Landsat and Sentinel-2 imagery, using Landsat 8 TOA reflectance as a benchmark [48].

The Normalized Burn Ratio (NBR) index, which has been widely used to detect forest disturbances due to its excellent sensitivity to chlorophyll in vegetation leaves, charcoal ash in soil, and moisture content, was selected for forest disturbance detection [11,49]. The NBR was calculated according to Equation (1):

$$NBR = \frac{\rho_{NIR} - \rho_{SWIR2}}{\rho_{NIR} + \rho_{SWIR2}} \tag{1}$$

where NIR and SWIR are the near-infrared (850–880 nm) and short-wave infrared (1570–1650 nm) bands of the Landsat and Sentinel-2 imagery, reflectively [50].

2.3.2. Forest Cover Data

This study is only concerned with the past disturbance history of existing forests. Prior to implementing the LandTrendr algorithm, non-forest was masked out using the 2020 forest map of Hainan Island to reduce the impact of other land sources, such as those used for crop planting and harvesting. The forest map was created using a decision tree algorithm developed with the Landsat/Sentinel-2 optical time series and L-band Phased Array L-band Synthetic Aperture Radar (PALSAR) and PALSAR-2 radar imagery [35,51]. The spatial distribution maps of forests on Hainan Island for 2007–2015 (OA = 92%–97%) were obtained using this algorithm, and its accuracy is significantly better than the existing forest products based on pure radar or optical remote sensing images in the region (OA = 82%–90%) [51]. It also maintains high spatial and temporal consistency at the one-year and five-year scales and is a reliable data product for dynamic forest monitoring in Hainan.

2.3.3. Terrain Data

The terrain data we used were from the Advanced Land Observing Satellite (ALOS) World 3D-30 m (AW3D30), a global digital surface model (DSM) provided by the Japan Aerospace Exploration Agency (JAXA). According to the topographic features of Hainan Island, the elevations were divided into seven levels with binning values of 50 m, 100 m, 200 m, 300 m, 600 m, and 1200 m. The slope was extracted from AW3D30 using the terrain analysis function on the GEE cloud platform. According to the technical regulations for the inventory for forest management planning and design (GB/T26424-2010) issued by the National Forestry and Grassland Administration of China, we classified slopes as shallow slopes (0–5°), gentle slopes (5–15°), slopes (15–25°), abrupt slopes (25–35°), steep slopes (35–45°), and dangerous slopes (≥45°). The spatial distribution and area of different forest disturbances at different elevation and slope regions were analyzed.

2.3.4. Verification Data

Based on the 2020 forest map, a total of 350 forest samples were randomly generated and visually interpreted using very high-resolution Google Earth imagery and historical thumbnails of Landsat imagery from the late 1980s onwards. These thumbnails were downloaded using a Python script developed with the functions of the geemap package The geemap package could be accessed from https://geemap.org/ (Accessed on 20 August 2022). Due to cloud cover and image quality, disturbances for some samples could not be determined, and ultimately only 334 samples were selected for subsequent analysis (there were 265 abrupt samples and 69 gradual samples) (Figure 1). These sample data were randomly selected in a ratio of 3:7, with 30% used as training samples and the remaining 70% used as accuracy assessment samples. Although multiple disturbances were identified as another type of disturbance, the lack of historical imagery did not permit the inclusion of this category in the visual interpretation of the disturbance samples.

2.4. Forest Disturbance Identification

The LandTrendr temporal segmentation algorithm is considered one of the best methods for effective forest disturbance monitoring [13,20]. The algorithm adapts a temporal segmentation method to capture long-lasting and short-term dramatic changes by analyzing the temporal spectral trajectory of each pixel. The input is an annual composite time series of spectral bands and/or spectral indices. The implementation of the LandTrendr algorithm consists of six main steps: (1) removing spikes (clouds, snow, smoke, or shadows); (2) identifying potential vertices; (3) fitting the trajectory; (4) simplifying the model; (5) determining the best model based on the p-value of the *F-test*; and (6) filtering the segments by comparing the segmented trajectory to the rate of change in vegetation cover [20].

To more accurately identify types and times of forest disturbance, we improved the final step of the LandTrendr algorithm (filtering segments by comparing segmentation trajectories with percent change in vegetation cover). Several metrics were calculated to describe forest disturbance: (1) number of segment vertices (N_{Vertex}); (2) value at the onset of disturbance (V_{start}); (3) value at disturbance end (V_{end}); (4) magnitude (V_{mag}); and (5) duration of disturbance (T_{dur}, Figure 3.). In this study, forest disturbances were classified as abrupt disturbance ($T_{dur} \leq 4$ years), gradual disturbance ($T_{dur} > 4$ years), multiple disturbance (number of disturbances >1), and no disturbance (Figure 4). The main steps are as follows: (1) determining the number of vertices and splitting them into two parts ($N_{Vertex} > 2$ and $N_{Vertex} = 2$); (2) for pixels with $N_{Vertex} > 2$, determining disturbance types (abrupt: $V_{start} \geq 0.6$, $V_{end} \leq 0.49$, and $V_{mag} \geq 0.18$; gradual: $V_{start} \geq 0.6$, $V_{end} \leq 0.53$, and $V_{mag} \geq 0.11$) according to the duration of the disturbance; (3) counting the number of disturbances and determining if it is a multiple disturbance; and (4) performing trend fitting for forest pixels with two vertices and categorizing them as increasing trend (slope ≥ 0) or decreasing trend (slope < 0). Thresholds of abrupt and gradual disturbance for V_{start}, V_{end}, and V_{mag} were determined using the training samples (V_{mag}: V_{mag} mean - V_{mag} standard deviation; V_{start}: V_{start} mean - V_{start} standard deviation; V_{end}: V_{end} mean + V_{end} standard deviation, Figure 5). Model performance was evaluated using a scatterplot of observed disturbance year against estimated disturbance year based on the validation dataset. All these processes were performed on the GEE cloud platform.

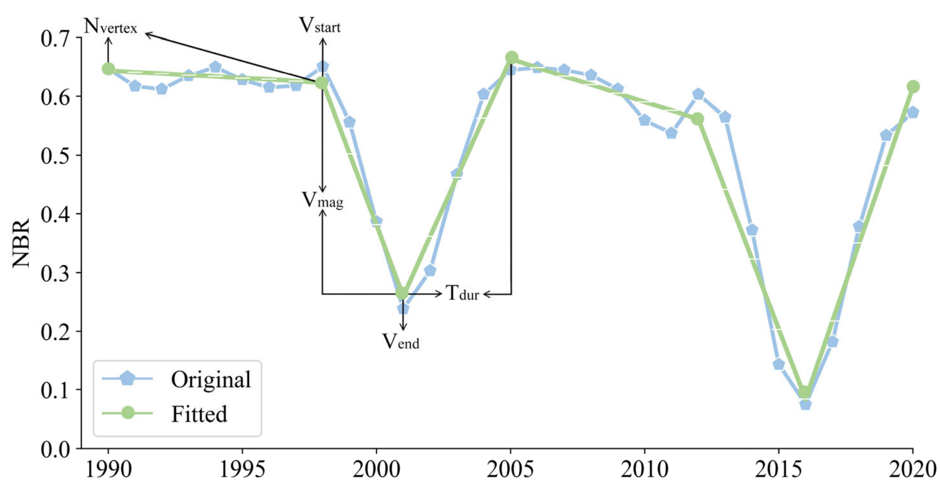

Figure 3. Metrics calculated for optimizing the LandTrendr algorithm.

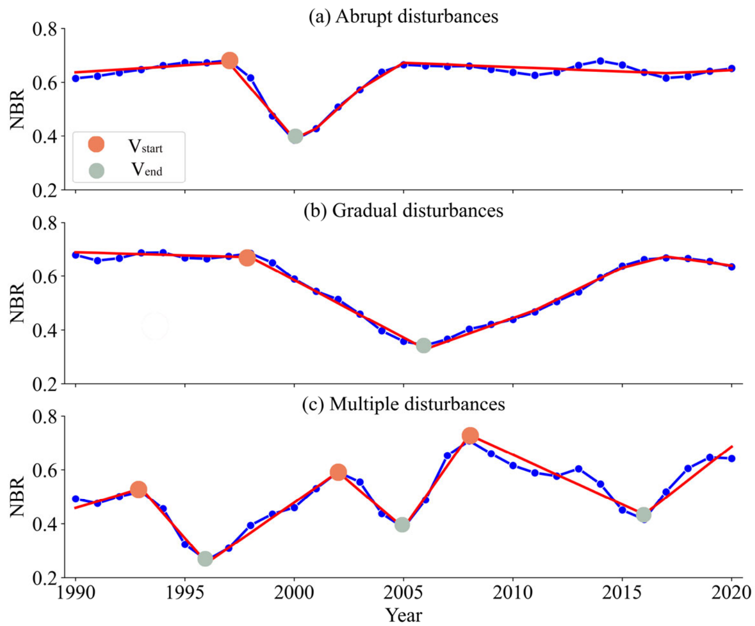

Figure 4. Types of forest disturbances in this study: (**a**) abrupt disturbances, (**b**) gradual disturbances, and (**c**) multiple disturbances.

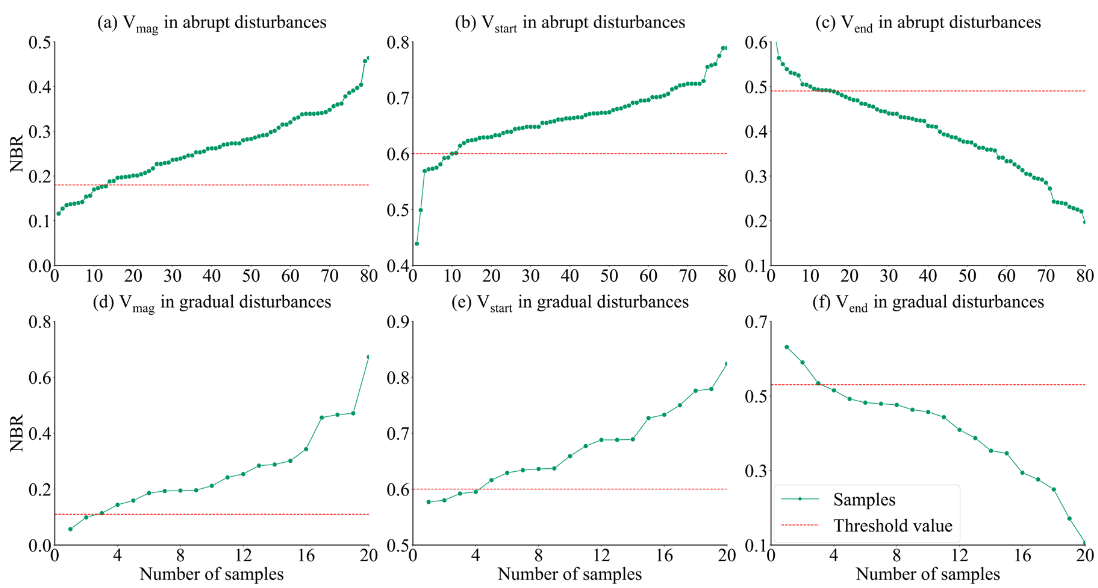

Figure 5. Threshold values for detecting abrupt and gradual disturbances: (**a**–**c**) V_{mag}, V_{start}, and V_{end} for abrupt disturbances, and (**d**–**f**) V_{mag}, V_{start}, and V_{end} for gradual disturbances. Th red dotted lines are the values of the corresponding mean ± standard deviation.

3. Results

3.1. Accuracy Assessment

Accuracy assessments of the disturbance date using 70% ground reference data for abrupt and gradual disturbances are shown, and the observed years and estimated years of the abrupt disturbances have clear linear distribution characteristics. The R^2 and slope of the linear fit are 0.92 and 0.95, respectively(Figure 6a). All points are closely distributed along the one-to-one line, but show a slight underestimation of the year of abrupt disturbances for most rubber plantations. The validation results for the gradual disturbances show a similar distribution pattern to those for the abrupt disturbances, with the R^2 and the slope of the linear fit reaching 0.84 and 0.83, respectively(Figure 6b). In contrast, the distribution of all points of the gradual disturbances is more discrete, and the algorithm underestimates the early gradual disturbances more.

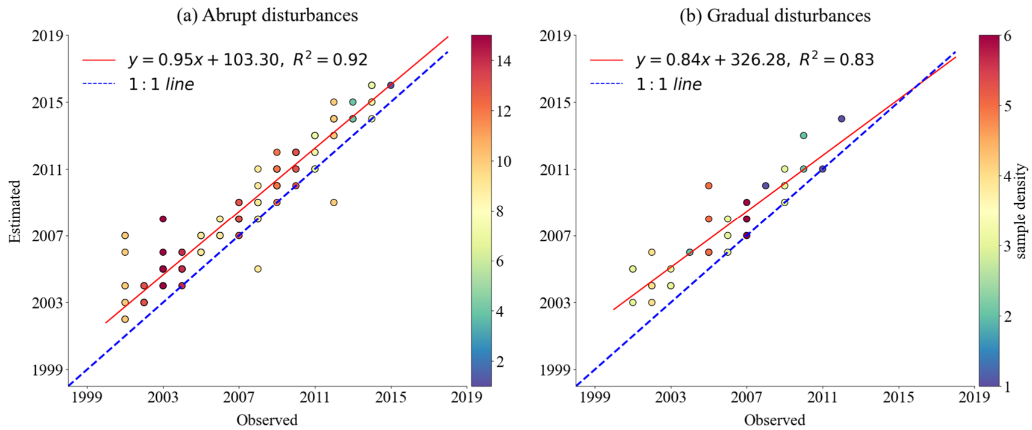

Figure 6. Scatter plots and linear fits of observed and estimated years of disturbances: (**a**) abrupt disturbances and (**b**) gradual disturbances.

3.2. Spatial Characteristics of Forest Disturbances on Hainan Island

3.2.1. Forest Disturbances over Different Cities and Counties

Abrupt disturbances are relatively concentrated in the central and northwestern regions, but the distribution varies greatly among different time periods (Figure 7a). Before 2000, abrupt disturbances occurred mainly in the central, western, and northwestern regions, especially in Danzhou City, Qiongzhong County, Baisha County, and Dongfang City. Between 2000 and 2010, abrupt disturbances increased significantly, and were mainly concentrated in the north-central and northwestern regions, particularly in Danzhou City, Qiongzhong County, Chengmai County, and Baisha County. After 2010, the area of abrupt disturbances decreased rapidly and became more prevalent in the central and northeastern regions.

Gradual disturbances are relatively scattered; they are distributed mainly in the northwestern region and the eastern coastal inland platform areas (Figure 7b). Before 2000, there were few gradual disturbances, mainly in the central and northwestern regions, such as Danzhou City, Baisha County, and Qiongzhong County. From 2001 to 2010, the gradual disturbances increased significantly and were concentrated in the northwestern, central-eastern, and northeastern regions. After 2010, the gradual disturbances gradually reduced in frequency and were mainly distributed in Danzhou City, Chengmai County, Qiongzhong County, and Baisha County.

Multiple disturbances have occurred in all cities and counties over the past three decades, but the area of disturbance is relatively small (Figure 7c). Multiple disturbances were concentrated in the western, northeastern, coastal, and central areas of Hainan Island. In contrast, the areas of multiple forest disturbances in Wenchang City, Qiongzhong County, and Dongfang City were much larger than in other cities and counties, such as Lingshui County, Ding'an County, and Chengmai County.

The area of forest disturbance on Hainan Island from 1990 to 2020 was 2.33×10^5 hm^2, which is about 10.84% of the forest area of Hainan Island in 2020 (2.15×10^6 hm^2) (Figure 7d). The areas of abrupt, gradual, and multiple disturbances were 1.21×10^5 hm^2 (51.93%), 9.96×10^4 hm^2 (42.75%), and 1.25×10^4 hm^2 (5.32%), respectively. Danzhou City had the largest area of abrupt disturbance (1.83×10^4 hm^2), followed by Qiongzhong County (1.62×10^4 hm^2), Baisha County (1.17×10^4 hm^2), and Chengmai County (1.02×10^4 hm^2). The areas of abrupt disturbances in these regions accounted for 46.63% of the total area of abrupt disturbances. In descending order, the top five cities and counties in terms of areas of gradual disturbances were Danzhou City (1.33 × 10^4 hm^2), Qiongzhong County (9.60 × 10^3 hm^2), Baisha County (9.33 × 10^3 hm^2), Qionghai City (7.74 × 10^3 hm^2), and Wenchang City (7.44 × 10^3 hm^2), accounting for 47.62% of the total area of gradual disturbances. In the case of multiple disturbances, Wenchang City hosted the largest area with 1.65 × 10^3 hm^2, followed by Qiongzhong County (1.42 × 10^3 hm^2) and Dongfang City (1.20 × 10^3 hm^2), which together accounted for 34.17% of the total area of multiple disturbances.

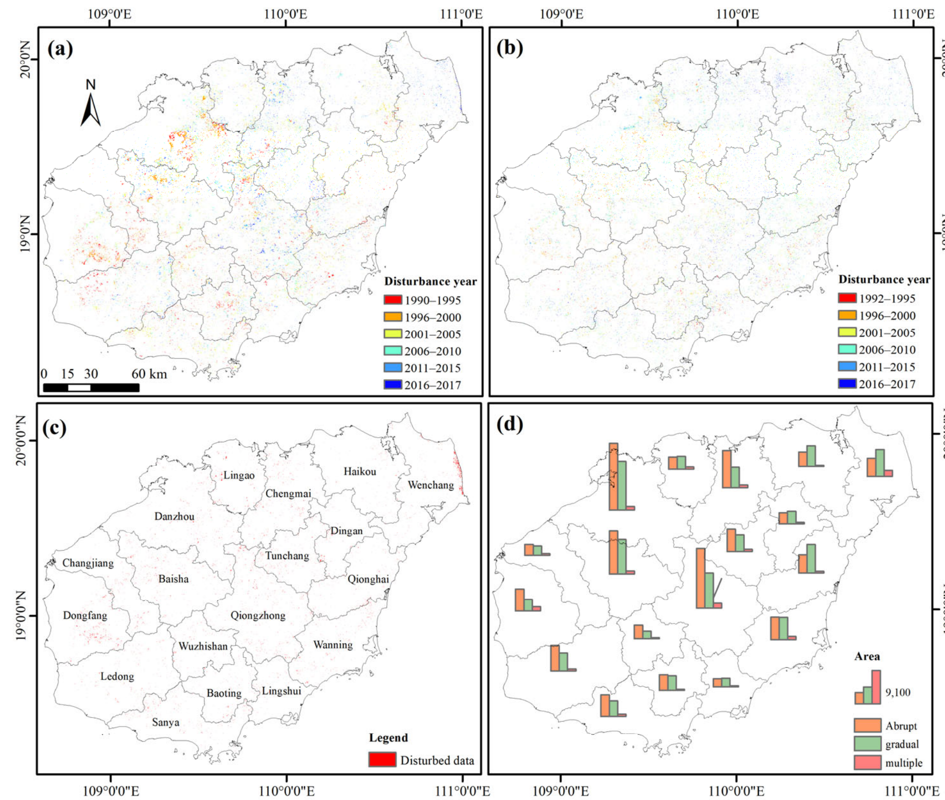

Figure 7. Spatial distributions of forest disturbances on Hainan Island from 1990 to 2020: (**a**) abrupt disturbances, (**b**) gradual disturbances, (**c**) multiple disturbances, and (**d**) areas of different disturbance types at city and county levels.

3.2.2. Forest Disturbances in Different Terrain Areas

Forest disturbances on Hainan Island in the past 30 years occurred mainly in the area below 600 m, and the area of disturbance varied greatly in different years (Figure 8a). In the 1990s, the area of forest disturbances increased most in the area with elevation between 100 m and 200 m, while most other areas increased only slightly. In the first five years of this century, the area of forest disturbances increased substantially, especially in areas less than 200 m in elevation. In 2005, the disturbed forest areas at elevations of 0–50 m, 50–100 m, and 100–200 m were 1.05 × 10^4 hm^2, 1.53 × 10^4 hm^2, and 2.32 × 10^4 hm^2, respectively. These increased by 3.43, 3.82, and 3.18 times the forest disturbance area in the early 1990s. After 2005, the area of forest disturbance began to decrease in most areas. By the end of 2020, the total area of forest disturbance below 600 m was about 2.27 × 10^5 hm^2, accounting for 97.42% of the total area of forest disturbance on Hainan Island. The largest area of forest disturbance was found an elevation of 100–200 m (7.52 × 10^4 hm^2) and accounted for 32.27% of the total forest disturbance area.

Forest disturbances on Hainan Island in the past 30 years were mainly distributed in areas with slopes below 25°, with the area below 15° changing the most (Figure 8b). The area of forest disturbance increased slowly in the 1990s, but increased significantly in the first five years of this century. The disturbed forest areas in the 0–5° and 5–15° regions were 2.45 × 10^4 hm^2 and 3.04 × 10^4 hm^2, respectively, which are about 3.60 and 3.00 times higher than those in the early 1990s. After 2005, the area of forest disturbance decreased in most areas. The total area of forest disturbance in areas with slopes less than 25° was 2.20 × 10^5 hm^2, accounting for 94.42% of the total area of forest disturbance. The largest forest disturbance area was found in areas with slopes between 5° and 15° (9.92 × 10^4 hm^2), which accounted for 42.58% of the total forest disturbance area.

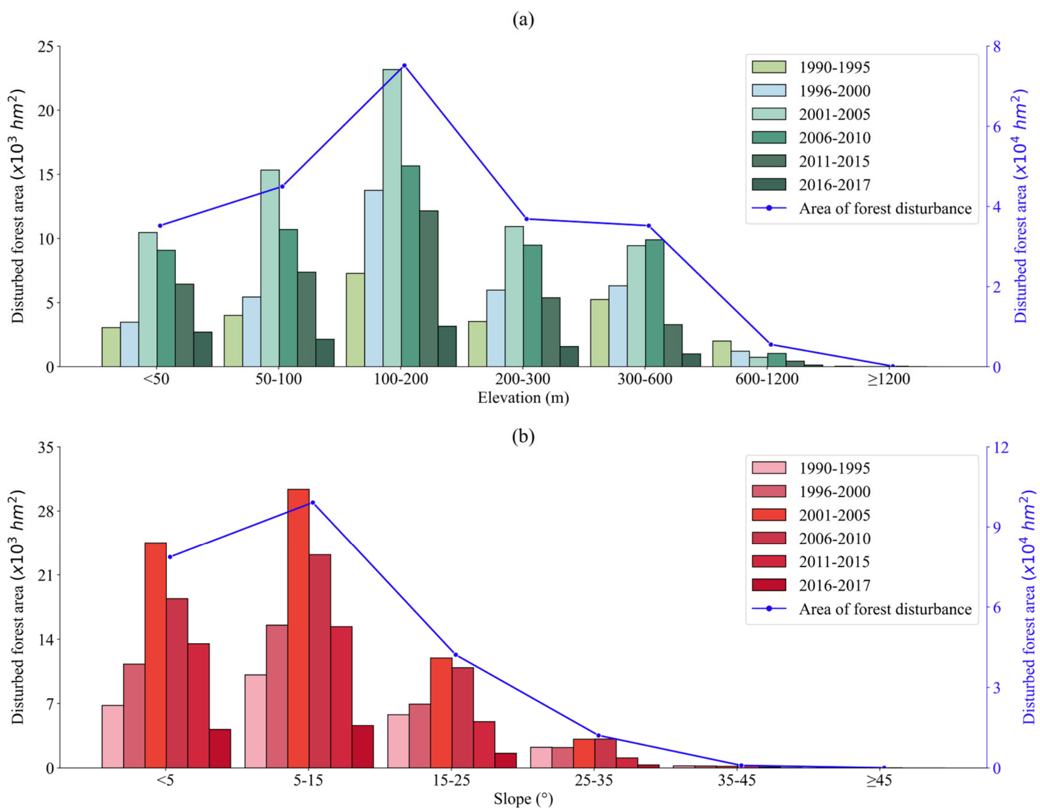

Figure 8. Areas of forest disturbance at different elevations and slopes on Hainan Island: (**a**) elevation and (**b**) slope.

3.3. Temporal Characteristics of Forest Disturbance

The areas of both abrupt and gradual disturbances showed a turning point around 2005: there was a general increase before 2005, and then a gradual decrease (Figure 9). Compared with the areas of abrupt disturbances, the areas of gradual disturbances increased more significantly before 2005 (Figure 9a) However, the magnitude of the decrease after 2005 was just the opposite, with gradual disturbances decreasing more rapidly. The year with the largest area of abrupt disturbances was 2005, with an area of 1.25 × 10^4 hm^2 and a 10.33% share of the total area of abrupt disturbances. The other years with large areas of abrupt disturbances were 2004, 2006, 2001, and 1996, with areas of 7.35 × 10^3 hm^2, 7.27 × 10^3 hm^2, 6.43 × 10^3 hm^2, and 6.31 × 10^3 hm^2, respectively. The total area of disturbances in these five years accounted for 32.94% of the total area of all abrupt disturbances. The largest area of gradual disturbances was found in 2006 (1.51 × 10^4 hm^2), which accounted for 15.16% of the total area of gradual disturbances. This was followed by 2007 (1.06 × 10^4 hm^2), 2005 (9.55 × 10^3 hm^2), 2004 (8.86 × 10^3 hm^2), and 2003 (6.45 × 10^3 hm^2). The total area of disturbance in these five years accounted for 50.76% of the total area of all gradual disturbances.

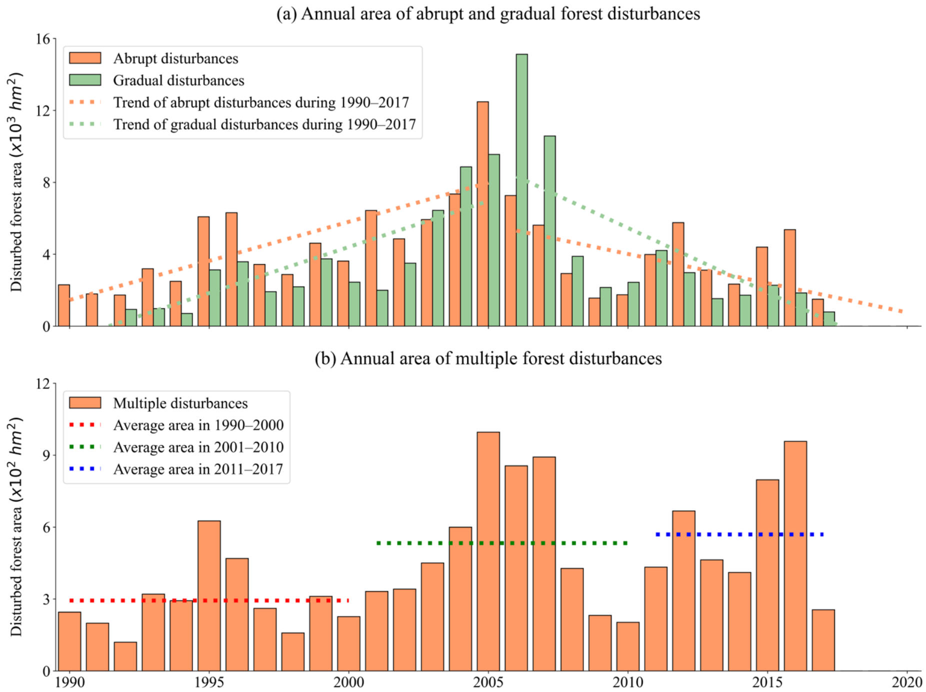

Figure 9. Interannual variation characteristics of forest disturbance: (**a**) abrupt and gradual disturbances, and (**b**) multiple disturbances.

The average annual area of multiple disturbances on Hainan Island was 293.76 hm^2 in 1990–2000, the lowest in the three decades(Figure 9b). From 2001 to 2010, the average annual disturbance area was 533.04 hm^2, which was a significant increase compared to 1990–2000. During this period, the disturbance area peaked between 2005 and 2007. The total area of multiple disturbances in these three years was 2744.00 hm^2, accounting for 51.48% of the total area of multiple disturbances in 2001–2010. The average annual disturbance area from 2010 to 2017 was 569.30 hm^2, which was slightly larger than the average disturbance area from 2001 to 2010. The disturbances mainly occurred in 2015 and 2016, and accounted for 44.03% of the area of multiple disturbances (3.98×10^3 hm^2) after 2010.

4. Discussion

4.1. Data and Algorithms for Forest Disturbance Monitoring

Satellite image quality is an important factor in forest disturbance monitoring. Landsat imagery has been used extensively for forest disturbance monitoring with the LandTrendr algorithm [11,52–54] because it has a long-term observation history [2]. However, the long-term monitoring of forest disturbances in the tropics with Landsat alone remains challenging due to frequent cloud cover [55]. In this study, both Landsat 5/7/8 and Sentinel-2 imagery was used to generate annual time series for forest disturbance monitoring. Although Sentinel-2 has only been in use since 2015, it effectively complements data from recent years. The results showed that the maximum revisit interval decreased to approximately seven days when Landsat 8 and Sentinel-2A/B were integrated [55]. The increasing amount of imagery data in recent years can provide more dynamic details and thus reduce the error in forest disturbance monitoring [56,57].

Although the LandTrendr algorithm has been used extensively to monitor forest disturbances, multiple disturbances are rarely observed [11,12,14,58]. In fact, forests are prone to multiple disturbances over a period of up to 30 years, especially in tropical regions where there are large numbers of fast-growing forests, such as eucalyptus. In this study, we successfully improved the LandTrendr algorithm to monitor multiple forest disturbances. As shown in Figure 10. ., multiple disturbances can be accurately identified using the time series trajectory fitted by the LandTrendr algorithm and verified with historical satellite imagery. The annual time series of the composite vegetation index shows that the NBR dropped to its lowest levels in 1995, 2007, and 2016 due to deforestation (Figure 10 c-e). The dates of the disturbances captured by LandTrendr's fitted time series trajectory were 1996, 2007, and 2016, respectively. Thumbnails of the historical images (Figure 10e) showed that disturbances occurred in 1996, 2006, and 2015, respectively. The comparison shows that the monitoring results differ by one year for two disturbances, which can be explained by the image composition method. Due to the relative scarcity of cloud-free imagery in the tropics, annual mosaic images was composited from satellite imagery from the previous year and the current year. Therefore, there is a one-year time shift of the NBR minimum value, which affects the fitting results of the LandTrendr algorithm.

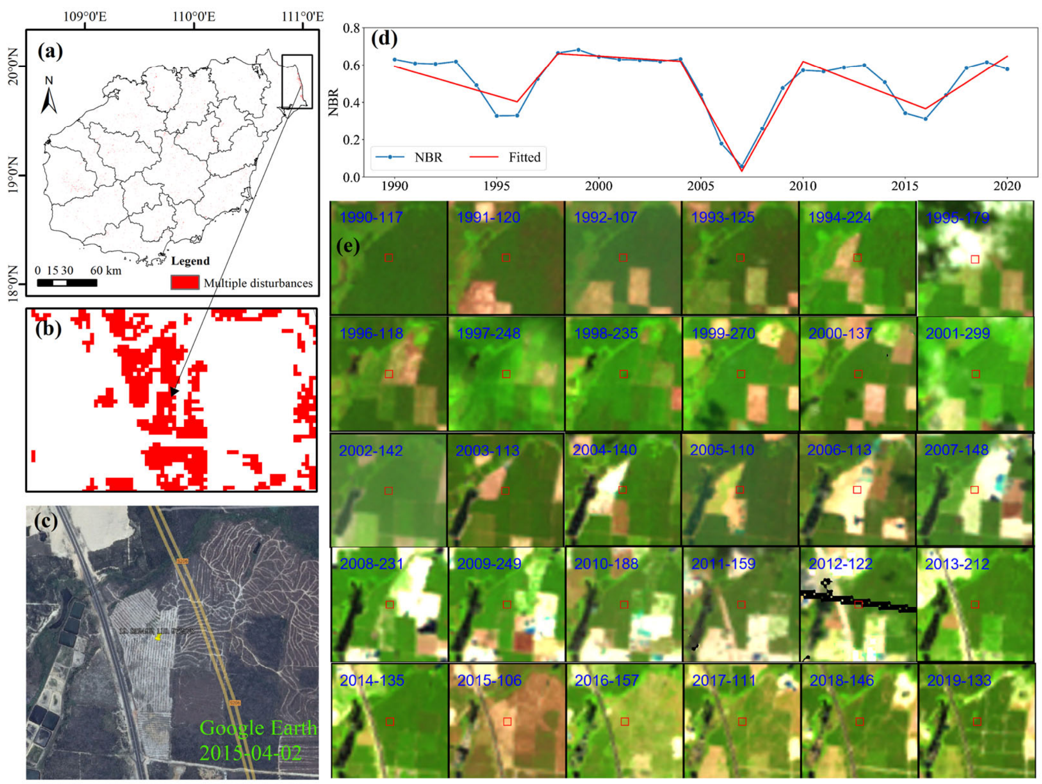

Figure 10. Schematic diagram of multiple forest disturbance monitoring: (**a**) map of multiple forest disturbances on Hainan Island, (**b**) zoom view of multiple forest disturbances along the coast of Wenchang City, (**c**) very high-resolution Google Earth satellite image of a typical disturbance area (110.97255° E, 19.85249° N), (**d**) corresponding annual NBR time series and fitted LandTrendr trajectory, and (**e**) thumbnails of historical satellite images.

4.2. Forest Disturbances on Hainan Island and Its Drivers

Our results show that the forest area of Hainan Island disturbed in the past 30 years is equivalent to 10.84% of the total forest area in 2020, with an average annual disturbance rate of 0.35%. The forest disturbance rate is lower than the 16.73% (0.64% per year) observed along the China–Laos border in 1991–2016 [27], and much lower than the 45% (3.46% per year) found along the Cambodia–Vietnam border in 2000–2012. Our results show that the forest area of Hainan Island disturbed in the past 30 years is equivalent to 10.84% of the total forest area in 2020, with an average annual disturbance rate of 0.35%. The forest disturbance rate is lower than the 16.73% (0.64% per year) observed along the China–Laos border in 1991–2016 [56], and much lower than the 45% (3.46% per year) found along the Cambodia–Vietnam border in 2000–2012. As a well-known global biodiversity hotspot, Hainan Island possesses many nature reserves, forest parks, and scenic areas from the local to the national level [59], and these effectively reduce human-induced forest disturbance. In addition, Hainan Province began to strengthen its forest protection and restoration in 1980, and logging of natural forests was completely banned in 1994, greatly improving forest cover [37].

The abrupt disturbances were mainly concentrated in the central and northwestern regions of Hainan Island, and they peaked around 2005. There are three main reasons for this spatiotemporal distribution. First, the development of the natural rubber industry. Rubber plantations have been established on Hainan Island since the 1950s, and it now host the second largest area of rubber plantations in China [60]. The first-generation rubber plantations continued to plant rubber trees (thus becoming second-generation rubber plantations) after they were cut down between the 1970s and 1990s. After 2000, the early second-generation rubber plantations were gradually deforested, and the planting of rubber trees continued. In particular, the rapid rise in rubber prices since 2003 promoted the rapid growth of rubber plantations [61]. According to the Statistical Yearbook of Hainan Island, the area of rubber plantations increased from 3.69×10^5 hm^2 in 1990 to 5.19×10^5 hm^2 in 2020 [39]. Rubber trees are arbor that are more than 20 m high, and the felling of rubber trees causes abrupt disturbances. Previous studies have shown that rubber plantations were distributed in all cities and counties on Hainan Island, but were more concentrated in the central, northwestern, and central-northern regions [35,36,51]. Second, the boom of pulp and paper forests, such as eucalyptus, since the 1990s. In 1992, Hainan Province began to promote the industrial cultivation of eucalyptus at the policy level, and the area of eucalyptus plantations increased significantly [62]. It was estimated that the area of eucalyptus plantations on Hainan Island was about 2×10^5 hm^2, mainly distributed in the northeast, northwest, and southwest regions [62]. The establishment of eucalyptus plantations and the harvesting of mature eucalyptus trees were most likely to cause abrupt disturbances [63]. Third, the expansion of orchards in the southern and southwestern regions. The southern regions, such as Sanya City and Linshui County, are among the true tropical regions with abundant sunlight and a warm climate all year round. The tropical fruits grown here can be marketed earlier and have higher yields [64,65]. Therefore, the first- and second-generation rubber plantations, and even some tropical forests in the southern region, have been gradually converted into tropical orchards, producing fruits such as mangoes, lychees, and longan, which have a forest character. According to the Hainan Island Statistical Yearbook, the area of orchards increased from 4.76×10^4 hm^2 in 1993 to 1.78×10^5 hm^2 in 2020 [39].

Gradual disturbances are relatively scattered, found mainly in the northwestern and eastern coastal inland platform areas, and these peaked around 2006. These disturbances were mostly caused by selective logging (e.g., pulp and paper forests) and severe natural disasters, such as typhoons and droughts [66,67]. Hainan Island lies in the path of typhoons and is therefore frequently hit by typhoons or tropical cyclones of varying intensity. From 1950 to 2019, there were 96 typhoons on Hainan Island, of which 67% landed on the east coast and northeast region [68,69]. Drought is another important disturbance factor. Hainan Island has distinct dry and rainy seasons, of which the rainy season from May to October accounts for more than 80% of annual rainfall [67]. In addition, the spatial heterogeneity of rainfall is large. The average annual rainfall in the driest western region is only about 941 mm, while the highest values in the central and eastern regions can be as high as 2388 mm [67]. The gradual disturbances that peaked around 2006 can be explained by two extreme natural disasters. First, the island experienced severe drought from the second half of 2004 to the first half of 2005, and then was hit by the destructive Typhoon Damrey in September 2005, the most severe since 1973 [70,71]. The monthly rainfall according to Climate Hazards Group InfraRed Precipitation with Station (CHIRPS) data for the entire island from September 2004 to June 2005 was well below the 40-year average monthly precipitation, with the largest deviation of about 90% occurring in October 2004 (precipitation <50 mm, Figure 11(a,b). Second, the subsequent Typhoon Damrey in September 2005 destroyed 50.9% of mature rubber plantations at a damage level of 3 and caused a total economic loss of USD 300 million to the Hainan State Farm Bureau rubber farming industry [66].

There are many cases of multiple disturbance throughout the island, but the distribution is relatively dense in the northeastern part of Wenchang City and the southern part of Dongfang City, peaking around 2005 and 2015. These disturbances were mostly caused by the repeated harvesting of pulp and paper forests. We overlaid the map and found that the multiple disturbance patches concentrated in the northeastern part of Wenchang were mainly located on the Daodong Forest Farm. On the one hand, the forest disturbances are due to historical logging of artificial forests, and on the other hand, they are influenced by typhoon disasters. For example, Super Typhoon Rammasun, one of the only three category 5 super typhoons recorded in the South China Sea, landed at peak intensity at the northeastern part of Wenchang City in 2014, hit the Daodong Forest Farm head-on, and caused destructive damage to about 7000 hectares of coastal protection forests [72,73]. The dense distribution of multiple disturbance patches in the southern part of Dongfang City is mainly due to the large area of eucalyptus forests.

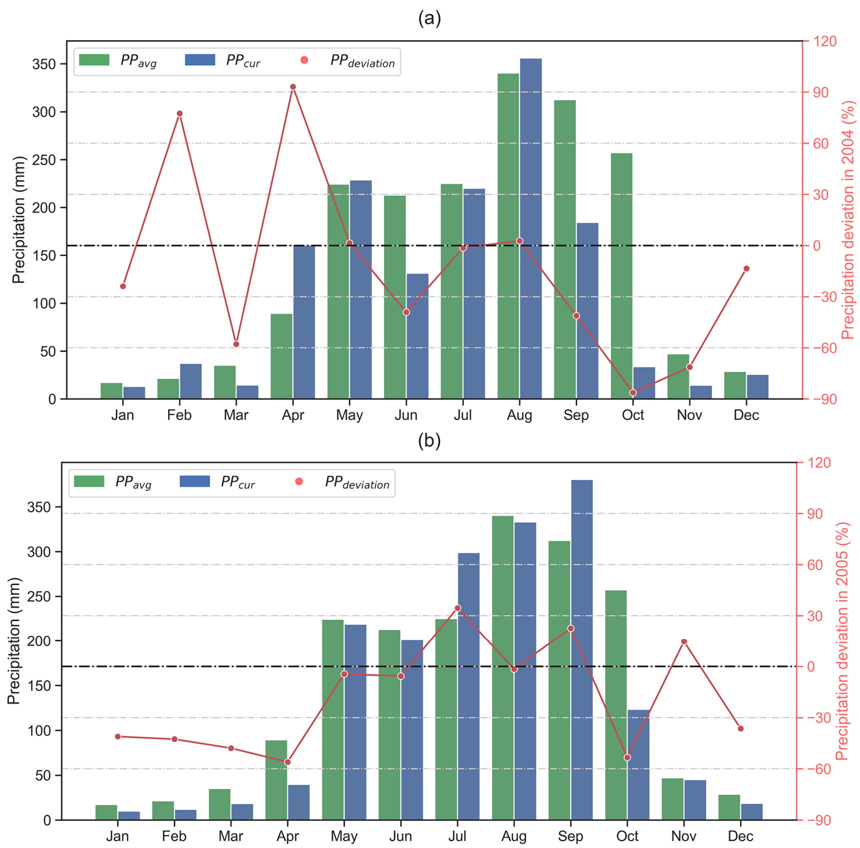

Figure 11. Monthly rainfall in 2004–2005 and its deviations from the 40-year average monthly rainfall on Hainan Island: (**a**) 2004 and (**b**) 2005. Results were analyzed using data from the Climate Hazards Group InfraRed Precipitation with Station (CHIRPS) on the GEE platform. (PP_{avg}: average precipitation 1981–2021, PP_{cur}: current year rainfall, $PP_{deviation}$: precipitation deviation).

5. Conclusions

In this study, we monitored forest disturbances on Hainan Island from 1987 to 2020 based on the Landsat and Sentinel-2 long time series datasets and the LandTrendr algorithm on the GEE platform.

We proposed a new LandTrendr algorithm that can better overcome the influence of cloudy and rainy weather as well as the complex landscape in tropical areas, and that can accurately identify abrupt disturbances, gradual disturbances, and multiple disturbances, with an R^2 ranging from 0.83 to 0.92. The analysis of the forest disturbance characteristics of Hainan Island shows that the forest disturbance on Hainan Island is relatively light, with an average annual disturbance ratio of only 0.35%. The forest disturbance is mainly in the central, northern, and northwestern regions. With regard to terrain, forest disturbances are concentrated at medium elevations and in areas with gentle topography, and few large forest disturbances occur at high elevations. In addition, forest disturbances were most frequent between 2000 and 2010, with the largest disturbance in 2005 caused by a combination of human-induced factors, such as the expansion of rubber, eucalyptus, and tropical fruit plantations, as well as natural disasters, such as Typhoon Damrey and drought.

Due to the large spatial heterogeneity of precipitation on Hainan Island, the NBR index of early planted eucalyptus trees fluctuates widely. In this study, the LandTrendr algorithm may not have been able to monitor the multiple disturbances caused by the rotational cycle of fast-growing forests such as eucalyptus, which may have led to an underestimation of the multi-turbulence area. Follow-up studies will attempt to further improve this algorithm to enhance the accuracy of multiple disturbance area extraction.

Author Contributions: Conceptualization, B.C. and W.K.; data curation, X.Y. and X.G.; formal analysis, X.Y. and H.L.; funding acquisition, B.C. and W.K.; investigation, X.Y., X.G., and Y.C.; resources, X.Y. and X.G.; supervision, Z.W. and T.Y.; writing—original draft, X.Y.; writing—review and editing, B.C. and W.K. All authors have read and agreed to the published version of the manuscript.

Funding: This research was funded in part by the National Natural Science Foundation of China (42071418,32260391), and the Natural Science Foundation of Hainan Province (2019RC329), The Youth Top Talents of Yunnan Ten Thousand Talents Program, Earmarked Fund for China Agriculture Research System (CARS-33), and the Natural Science Foundation of Jiangsu Province (BK20221337).

Institutional Review Board Statement: Not applicable.

Informed Consent Statement: Not applicable.

Data Availability Statement: Not applicable.

Acknowledgments: The author would like to thank Google Earth Engine (GEE) for providing free satellite imagery data and providing a large amount of data support for this study. The relevant data of this study is obtained through this website (https://code.earthengine.google.com/ accessed on 3 October 2021).

Conflicts of Interest: The authors declare no conflict of interest.

References

1. Gasparri, N.I.; Grau, H.R. Deforestation and fragmentation of Chaco dry forest in NW Argentina (1972–2007). *For. Ecol. Manag*. **2009**, *258*, 913–921.
2. Liu, S.; Wei, X.; Li, D.; Lu, D. Examining Forest Disturbance and Recovery in the Subtropical Forest Region of Zhejiang Province Using Landsat Time-Series Data. *Remote Sens*. **2017**, *9*, 479.
3. Potapov, P.V.; Turubanova, S.A.; Adusei, B.; Broich, M.; Altstatt, A.; Mane, L.; Justice, C.O. Quantifying forest cover loss in Democratic Republic of the Congo, 2000–2010, with Landsat ETM+ data. *Remote Sens. Environ*. **2012**, *122*, 106–116.
4. Pan, Y.; Birdsey, R.A.; Fang, J.; Houghton, R.; Kauppi, P.E.; Kurz, W.A.; Phillips, O.L.; Shvidenko, A.; Lewis, S.L.; Canadell, J.G.; et al. A large and persistent carbon sink in the world's forests. *Science* **2011**, *333*, 988–993.
5. Brooks, T.M.; Mittermeier, R.A.; Mittermeier, C.G.; Da Fonseca, G.A.B.; Rylands, A.B.; Konstant, W.R.; Flick, P.; Pilgrim, J.; Oldfield, S.; Magin, G.; et al. Habitat Loss and Extinction in the Hotspots of Biodiversity. *Conserv. Biol*. **2002**, *16*, 909–923.
6. Jarron, L.; Hermosilla, T.; Coops, N.; Wulder, M.; White, J.; Hobart, G.; Leckie, D. Differentiation of Alternate Harvesting Practices Using Annual Time Series of Landsat Data. *Forests* **2017**, *8*, 15.
7. Wei, X.; Blanco, J.A. Significant Increase in Ecosystem C Can Be Achieved with Sustainable Forest Management in Subtropical Plantation Forests. *PLoS ONE* **2014**, *9*, e89688.
8. Bowd, E.J.; Banks, S.C.; Bissett, A.; May, T.W.; Lindenmayer, D.B. Direct and indirect disturbance impacts in forests. *Ecol. Lett*. **2021**, *24*, 1225–1236.
9. Portillo-Quintero, C.; Hernández-Stefanoni, J.L.; Reyes-Palomeque, G.; Subedi, M.R. The Road to Operationalization of Effective Tropical Forest Monitoring Systems. *Remote Sens.* **2021**, *13*, 1370.

10. Pflugmacher, D.; Cohen, W.B.; Kennedy, R.E. Using Landsat-derived disturbance history (1972–2010) to predict current forest structure. *Remote Sens. Environ*. **2012**, *122*, 146–165.
11. Schneibel, A.; Stellmes, M.; Röder, A.; Frantz, D.; Kowalski, B.; Haß, E.; Hill, J. Assessment of spatio-temporal changes of smallholder cultivation patterns in the Angolan Miombo belt using segmentation of Landsat time series. *Remote Sens. Environ*. **2017**, *195*, 118–129.
12. Li, Y.; Wu, Z.; Xu, X.; Fan, H.; Tong, X.; Liu, J. Forest disturbances and the attribution derived from yearly Landsat time series over 1990–2020 in the Hengduan Mountains Region of Southwest China. *For. Ecosyst*. **2021**, *8*, 73.
13. Senf, C.; Pflugmacher, D.; Wulder, M.; Hostert, P. Characterizing spectral-temporal patterns of defoliator and bark beetle disturbances using Landsat time series. *Remote Sens. Environ*. **2015**, *170*, 166–177.
14. Marzo, T.D.; Gasparri, N.I.; Lambin, E.F.; Kuemmerle, T. Agents of Forest Disturbance in the Argentine Dry Chaco. *Remote Sens.* **2022**, *14*, 1758.
15. Schwantes, A.M.; Swenson, J.J.; Jackson, R.B. Quantifying drought-induced tree mortality in the open canopy woodlands of central Texas. *Remote Sens. Environ*. **2016**, *181*, 54–64.
16. Meigs, G.W.; Kennedy, R.E.; Cohen, W.B. A Landsat time series approach to characterize bark beetle and defoliator impacts on tree mortality and surface fuels in conifer forests. *Remote Sens. Environ*. **2011**, *115*, 3707–3718.
17. Griffiths, P.; Kuemmerle, T.; Kennedy, R.E.; Abrudan, I.V.; Knorn, J.; Hostert, P. Using annual time-series of Landsat images to assess the effects of forest restitution in post-socialist Romania. *Remote Sens. Environ*. **2012**, *118*, 199–214.
18. Yan, G.; Solórzano, J.V.; Quevedo, A.; Loya-Carrillo, J.O. How BFAST Trend and Seasonal Model Components Affect Disturbance Detection in Tropical Dry Forest and Temperate Forest. *Remote Sens*. **2021**, *13*, 2033.
19. Kennedy, R.E.; Yang, Z.; Cohen, W.B.; Pfaff, E.; Braaten, J.; Nelson, P. Spatial and temporal patterns of forest disturbance and regrowth within the area of the Northwest Forest Plan. *Remote Sens. Environ*. **2012**, *122*, 117–133.
20. Kennedy, R.E.; Yang, Z.; Cohen, W.B. Detecting trends in forest disturbance and recovery using yearly Landsat time series:LandTrendr-Temporal segmentation algorithms. *Remote Sens. Environ*. **2010**, *114*, 2897–2910.
21. Huang, C.; Goward, S.N.; Masek, J.G.; Thomas, N.; Zhu, Z.; Vogelmann, J.E. An automated approach for reconstructing recent forest disturbance history using dense Landsat time series stacks. *Remote Sens. Environ*. **2010**, *114*, 183–198.
22. Verbesselt, J.; Zeileis, A.; Herold, M. Near real-time disturbance detection using satellite image time series. *Remote Sens. Environ*. **2012**, *123*, 98–108.
23. Zhu, Z.; Woodcock, C.E. Continuous change detection and classification of land cover using all available Landsat data. *Remote Sens. Environ*. **2014**, *144*, 152–171.
24. Zhu, Z. Change detection using landsat time series: A review of frequencies, preprocessing, algorithms, and applications. *Isprs. J. Photogramm*. **2017**, *130*, 370–384.
25. Ju, J.; Roy, D.P. The availability of cloud-free Landsat ETM+ data over the conterminous United States and globally. *Remote Sens. Environ*. **2008**, *112*, 1196–1211.
26. Cohen, W.B.; Yang, Z.; Healey, S.P.; Kennedy, R.E.; Gorelick, N. A LandTrendr multispectral ensemble for forest disturbance detection. *Remote Sens Environ*. **2018**, *205*, 131–140.
27. Tang, D.; Fan, H.; Yang, K.; Zhang, Y. Mapping forest disturbance across the China-Laos border using annual Landsat time series. *Int. J. Remote. Sens*. **2019**, *40*, 2895–2915.
28. Yang, Y.; Peter, D.E.; Alex, M.L.; David, M.; Zhang, S.; Zhenyu, W. Detecting the dynamics of vegetation disturbance and recovery in surface mining area via Landsat imagery and LandTrendr algorithm. *J. Clean. Prod*. **2018**, *178*, 353–362.
29. Kennedy, R.; Yang, Z.; Gorelick, N.; Braaten, J.; Cavalcante, L.; Cohen, W.; Healey, S. Implementation of the LandTrendr Algorithm on Google Earth Engine. *Remote Sens.* **2018**, *10*, 691.
30. Shao, Z.; Cai, J.; Fud, P.; Hu, L.; Liu, T. Deep learning-based fusion of Landsat-8 and Sentinel-2 images for a harmonized surface reflectance product. *Remote Sens. Environ*. **2019**, *235*, 111425.
31. Claverie, M.; Junchang, J.; Jeffrey, G.M.; Jennifer, L.D.; Eric, F.V.; Roger, J.; Sergii, V.S.; Christopher, J. The Harmonized Landsat and Sentinel-2 surface reflectance data set. *Remote Sens. Environ*. **2018**, *219*, 145–161.
32. Schiberna, E.; Borovics, A.; Benke, A. Economic Modelling of Poplar Short Rotation Coppice Plantations in Hungary. *Forests* **2021**, *12*, 623.
33. Temesgen, D.; Gonzálo, J.; Turrión, M.B.; Tunney, H. Effects of short-rotation Eucalyptus plantations on soil quality attributes in highly acidic soils of the central highlands of Ethiopia. *Soil Use Manag*. **2016**, *32*, 210–219.
34. Pasquarella, V.J.; Evalo, P.A.; Bratley, K.H.; Bullock, E.L.; Gorelick, N.; Yang, Z.; Kennedy, R.E. Demystifying LandTrendr and CCDC temporal segmentation. *Int. J. Appl. Earth Obs. Geoinf.* **2022**, *110*, 102806.
35. Gu, X.; Chen, B.; Yun, T.; Li, G.; Wu, Z.; Kou, W. Spatio-temporal Changes of Forest in Hainan Island from 2007 to 2018 Based on Multi-source Remote Sensing Data. *Chin. J. Trop. Crops* **2022**, *43*, 418–429.
36. Li, G.; Weili, K.; Zhixiang, W.; Xicai, Z.; Ting, Y.; Jun, M.; Rui, S.; Ying, L.; Bangqian, C. Spatio-temporal changes of rubber plantations in Hainan Island over the past 30 years. *J. Nanjing For. Univ.* **2022**, 1–11.
37. Huang, J. Study on Sustainable Management of Tropical Forests in Hainan Island, China. Ph.D. Thesis, Chinese Academy of Forestry, Beijing, China, 2006.
38. Zhu, M.; Wang, X.; Wang, S.; Wang, W.; Zou, Y.; Liang, Q. Carbon storage and distribution of rubber and eucalyptus plantations in Danzhou, Hainan Island. *Ecol. Sci.* **2016**, *35*, 43–51.
39. Hainan Provincial Bureau of Statistics. In *Hainan Statistical Yearbook*; China Statistics Press: Beijing, China, 2020.

40. Wang, S.; Ouyang, Z.; Zhang, C.; Xu, W.; Xiao, Y. The dynamics of spatial and temporal changes to forested land and key factors driving change on Hainan Island. *Acta Ecol. Sin.* **2012**, *32*, 7364–7374.
41. Chen, B.; Li, X.; Kou, W.; Qin, Y.; Yang, C.; Xie, G. Mapping tropical forests and deciduous rubber plantations in Hainan Island, China by integrating PALSAR 25-m and multi-temporal Landsat images. *Int. J. Appl. Earth Obs*. **2016**, *50*, 117–130.
42. Hermosilla, T.; Wulder, M.A.; White, J.C.; Coops, N.C. Prevalence of multiple forest disturbances and impact on vegetation regrowth from interannual Landsat time series (1985–2015). *Remote Sens. Environ*. **2019**, *233*, 111403.
43. Vogelmann, J.E.; Gallant, A.L.; Shi, H.; Zhu, Z. Perspectives on monitoring gradual change across the continuity of Landsat sensors using time-series data. *Remote Sens. Environ*. **2016**, *185*, 258–270.
44. Hislop, S.; Haywood, A.; Alaibakhsh, M.; Nguyen, T.H.; Soto-Berelov, M.; Jones, S.; Stone, C. A reference data framework for the application of satellite time series to monitor forest disturbance. *Int. J. Appl. Earth Obs*. **2021**, *105*, 102636.
45. Xi, Z.; Lu, D.; Liu, L.; Ge, H. Detection of Drought-Induced Hickory Disturbances in Western Lin An County, China, Using Multitemporal Landsat Imagery. *Remote Sens.* **2016**, *8*, 345.
46. Quintero, N.; Viedma, O.; Urbieta, I.R.; Moreno, J.M. Assessing Landscape Fire Hazard by Multitemporal Automatic Classification of Landsat Time Series Using the Google Earth Engine in West-Central Spain. *Forests* **2019**, *10*, 518.
47. Zhu, Z.; Wang, S.; Woodcock, C.E. Improvement and expansion of the Fmask algorithm: Cloud, cloud shadow, and snow detection for Landsats 4 – 7, 8, and Sentinel 2 images. *Remote Sens. Environ*. **2015**, *159*, 269–277.
48. Chastain, R.; Housman, I.; Goldstein, J.; Finco, M. Empirical cross sensor comparison of Sentinel-2A and 2B MSI, Landsat-8 OLI, and Landsat-7 ETM+ top of atmosphere spectral characteristics over the conterminous United States. *Remote Sens. Environ*. **2019**, *221*, 274–285.
49. White, J.C.; Wulder, M.A.; Hermosilla, T.; Coops, N.C.; Hobart, G.W. A nationwide annual characterization of 25 years of forest disturbance and recovery for Canada using Landsat time series. *Remote Sens. Environ*. **2017**, *194*, 303–321.
50. Escuin, S.; Navarro, R.; Fernández, P. Fire severity assessment by using NBR (Normalized Burn Ratio) and NDVI (Normalized Difference Vegetation Index) derived from LANDSAT TM/ETM images. *Int. J. Remote Sens*. **2008**, *29*, 1053–1073.
51. Chen, B.; Xiao, X.; Ye, H.; Ma, J.; Doughty, R.; Li, X.; Zhao, B.; Wu, Z.; Sun, R.; Dong, J.; et al. Mapping Forest and Their Spatial-Temporal Changes From 2007 to 2015 in Tropical Hainan Island by Integrating ALOS/ALOS-2 L-Band SAR and Landsat Optical Images. *Ieee J-Stars*. **2018**, *11*, 852–867.
52. Gelabert, P.J.; Rodrigues, M.; de la Riva, J.; Ameztegui, A.; Sebastià, M.T.; Vega-Garcia, C. LandTrendr smoothed spectral profiles enhance woody encroachment monitoring. *Remote Sens. Environ*. **2021**, *262*, 112521.
53. Jutras-Perreault, M.; Gobakken, T.; Ørka, H.O. Comparison of two algorithms for estimating stand-level changes and change indicators in a boreal forest in Norway. *Int. J. Appl. Earth Obs*. **2021**, *98*, 102316.
54. Zhu, L.; Liu, X.; Wu, L.; Tang, Y.; Meng, Y. Long-Term Monitoring of Cropland Change near Dongting Lake, China, Using the LandTrendr Algorithm with Landsat Imagery. *Remote Sens.* **2019**, *11*, 1234.
55. Li, J.; Roy, D.P. A Global Analysis of Sentinel-2A, Sentinel-2B and Landsat-8 Data Revisit Intervals and Implications for Terrestrial Monitoring. *Remote Sens*. **2017**, *9*, 902.
56. Curtis, E.W.; Thomas, R.L.; Martin, H.; Marvin, E.B. Transitioning from change detection to monitoring with remote sensing: A paradigm shift. *Remote Sens. Environ*. **2020**, *238*, 111558.
57. Shimizu, K.; Ota, T.; Mizoue, N. Detecting Forest Changes Using Dense Landsat 8 and Sentinel-1 Time Series Data in Tropical Seasonal Forests. *Remote Sens.* **2019**, *11*, 1899.
58. Hua, J.; Chen, G.; Yu, L.; Ye, Q.; Jiao, H.; Luo, X. Improved Mapping of Long-Term Forest Disturbance and Recovery Dynamics in the Subtropical China Using All Available Landsat Time-Series Imagery on Google Earth Engine Platform. *IEEE J. Sel. Top. Appl. Earth Obs. Remote Sens.* **2021**, *14*, 2754–2768.
59. Grogan, K.; Dirk, P.; Patrick, H.; Robert, K.; Rasmus, F. Cross-border forest disturbance and the role of natural rubber in mainland Southeast Asia using annual Landsat time series. *Remote Sens. Environ*. **2015**, *169*, 438–453.
60. Liu, R. Historical Analysis of China's Natural Rubber Industry. *China State Farm*. **2016**, *7*, 36–39.
61. Mo, Y. Natural rubber production and market situation. *World Trop. Agric. Inf.* **2012**, *5*, 1–3.
62. Li, Q. Research on the Development Countermeasures of Hainan Eucalyptus Industry. *Trop. Agric. Guangxi* **2010**, *3* ,51–54.
63. Ma, Y.; Fan, S.; Liu, Q.; Liu, H. Analysis of Forest Resource Dynamics in Hainan Province. *J. Anhui Agric. Sci.* **2012**, *40*, 14295–14299.
64. Tian, X. Exploration on the Development of Hainan New Tropical Leisure Orchard. *Xiandai Hortic.* **2011**, *5*, 22–23.
65. Zhu, J. Present Situation, Problems and Development Suggestions of Hainan Mango Industry. *Agric. Eng. Technol.* **2019**, *39*, 20–21.
66. Yu, W.; Zhang, M.; Mai, Q.; Jiang, J. Damage of Typhoon Damrey to the Rubber Industry in Hainan State Farm Bureau and Its Countermeasures for Future Development. *Chin. J. Trop. Agric.* **2006**, *26*, 41–43.
67. Li, W.; Zhang, J.; Liu, S.; Che, X.; Chen, X.; Zou, H. Meteorological characteristics and monitoring index of drought in Hainan Island. *J. Trop. Biol.* **2022**, *13*, 324–330.
68. Chen, Y. Risk assessment of typhoon disaster in Hainan Island based on GIS. Bachelor's Thesis, Chongqing Jiaotong University, Chongqing, China, 2021.
69. Chen, X.; Li, W.; Liang, C.; Bai, R.; Wu, H. Major agrometeorological disasters in Hainan and their control. *J. Trop. Biol.* **2022**, *13*, 416–421.
70. Yu, S.; Zhai, P.; Zhang, Q. Variation of Char acteristics of Drought in Hainan Island during 1961. *Chin. J. Trop. Crops* **2006**, *27*, 111–115.
71. Zhang, C.; Wu, S. Analysis on the Effect of High Temperature on Drought in Southwestern Hainan Island. *Adv. Meteorol. Sci. Technol.* **2020**, *10*, 96–101.

72. Xue, Y.; Yang, Z.; Chen, Y.; Wang, X.; Wu, S.; Huang, G.; Lin, Z. Typhoon 'rammasun' impact on forest ecosystem in hainan. *Trop. For.* **2014**, *42*, 34–38.
73. Ma, J.; Yang, W. Difference Analysis of Storm Surge between Typhoon Kalmaegi and Rammasun. *Guangdong Water Resour. Hydropower* **2015**, *112*, 20–24.